A Tactile Sensor Sheet Using Pressure Conductive Rubber With Electrical-Wires Stitched Method

Makoto Shimojo, Akio Namiki, Masatoshi Ishikawa, Ryota Makino, and Kunihiko Mabuchi

***Abstract*—A new type of tactile sensor using pressure-conductive rubber with stitched electrical wires is presented. The sensor is thin and flexible and can cover three-dimensional objects. Since the sensor adopts a single-layer composite structure, the sensor is durable with respect to external force. In order to verify the effectiveness of this tactile sensor, we performed an experiment in which a four-fingered robot hand equipped with tactile sensors grasped sphere and column. The sensor structure, electrical circuit, and characteristics are described. The sensor control system and experimental results are also described.**

***Index Terms*—Flexible sensor, pressure-conductive rubber, tactile sensor, wire stiching.**

I. Introduction

RECENTLY, the achievement of a robot that coexists with humans has become a reality. The development of the tactile sensor of the robot that can be used to cover the whole body is one of the key technologies. The tactile sensor will make the robot operate in unstructured environments, among people, among obstacles, under sea, or faraway planets. The tactile sensor will make the robots "cautious" and, thus, friendly to their environments [1]. Up until now, a large number of experimental devices and prototypes have been built and reported in the literature. However, the literature reveals very few applications beyond the experimental prototype stage, and hardly any applications are in serious regular use [2], [3]. This is due partly to the difficulty of making the tactile sensor and partly to the lack of availability of a sensor with suitable configurations and characteristics [3]. Important configurations of the tactile sensor include being thin and flexible. Because a robot hand usually has mechanical parts and wires inside its fingers and palm, it is necessary to attach a tactile sensor only on the surface of the hand. In addition, since the fingers have a curved surface, the sensor must be flexible. Also, it is preferable that the tactile sensor covers the whole body of the robot, like sensitive skin. Therefore, extensive surface sensing is desirable in a tactile sensor.

Inaba *et al.* developed a full-body sensing suit for a small robot [4]. The sensor suit was designed to be soft and flexible by using electrically conductive fabric and string. This method is very interesting and practical. The measuring principle is that the spacer is held between a sheet of electrically conductive fabric, and the contact resistance value between the fabric by the pressure is measured. The wires from the sensing element use the electrically conductive fiber. The problem with this design is that the number of wires from the sensing elements must equal the number of sensing elements. Thus, the number of wires becomes large when a wide area is covered. Another disadvantage is that the pressure-sensitive characteristic becomes almost ON/OFF. Lumelsky *et al.* also developed sensitive skin that contains 8×8 active infrared sensor pairs (i.e., LED + photo detectors), each of which can sense objects [1]. Since the reflection of light is used, proximity distance sensing is possible, and collision prevention is effective. However, in its present state, the detector is arranged at 25-mm intervals, and a high-density arrangement may be difficult to make. The Tekscan company manufactures a sensing sheet using arrays of pressure-sensitive resistor elements [5]. The Interlink company has developed a force-sensing resistor (FRS) [6]. FSR is available for use in experimental tactile sensor systems. The sensing elements of Tekscan and FSR are printed on thin films. The film is a pliable sheet, but it is not elastic. The film can cover a three-dimensional (3-D) surface with a two-dimensional expansion plane. However, this means that the film, because it is pliable but not elastic, cannot exactly cover a free-form 3-D object. Shinoda *et al.* developed a sensitive skin using wireless tactile sensing chips [7]. Many sensing chips are scattered within an elastic body which covers a wide robot surface. This method is very interesting. However, these are prototypes which have not been used in a practical application.

This paper discusses a tactile sensor that is thin and flexible and able to attach to a curved surface. In addition, this paper describes the principles, structure, and characteristics of the developed tactile sensor, and then presents experimental results.

II. Principle and Structure of Sensor

Fig. 1 shows a robot hand with the developed tactile sensors. The tactile sensor is attached to four fingers and covered with a silicon rubber film in order to prevent the sensor from wear by contact or chemical contamination. This first section describes the principles and structure of this tactile sensor.

A. Pressure Sensitive Material

This sensor uses pressure conductive rubber as a pressure-sensitive material. Pressure-conductive rubber has many excellent features, such as flexibility, workability, and ease of making thin films. The rubber (the product of Yokohama Rubber Co.,

Manuscript received October 29, 2002; revised October 21, 2003. The associate editor coordinating the review of this paper and approving it for publication was Dr. H. Troy Nagle.

M. Shimojo and R. Makino are with Mechanical Engineering and Intelligent Systems, The University of Electro-Communications, Tokyo 182-8585, Japan (e-mail: shimojo@mce.uec.ac.jp; ryota@rm.mce.uec.ac.jp).

A. Namiki, M. Ishikawa, and M. Mabuchi are with the Department of Information Physics and Computing, Graduate School of Information Science and Technology, University of Tokyo, Tokyo 113-8656, Japan (e-mail: namik@k2.t.u-tokyo.ac.jp; ishikawa@k2.t.u-tokyo.ac.jp; mabuchi@ccr.u-tokyo.ac.jp).

Digital Object Identifier 10.1109/JSEN.2004.833152

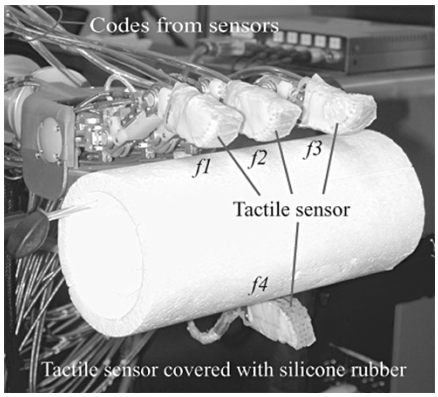

Fig. 1. Four-fingered hand with tactile sensors. The tactile sensors were mounted on the tips of each finger. The sensors were covered with thin, silicone rubber film.

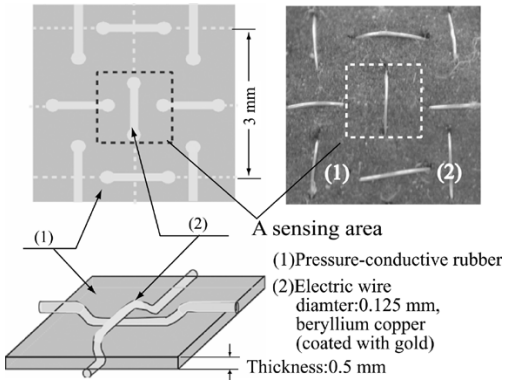

Fig. 2. Structure of a sensing element. Wires were stitched into the pressure-conductive rubber.

Ltd.) consists of carbon particles, which function as electroconductive material and are dispersed uniformly in a silicone rubber matrix. The electricity-conducting mechanism of pressure-conductive rubber seems to be due to the following principle. In the state without pressure, the carbon particles are positioned apart from each other; consequently, the resistance value is infinitely large. However, when pressure is applied, the thickness of the rubber decreases, and carbon particles form a chain of contact: This brings about a reduction in resistance value.

B. Conventional Sensor Structure

One conventional type of sensor structure is rubber that is attached to a substrate, on which electrodes are printed in a comb-like design [8]. The contact force is measured by the resistance between electrodes, which counter each other like the blades of a comb. Although this method can produce a very dense, thin tactile sensor, peeling of the rubber from the electrodes may occur due to the force in the tangential direction; sensor deformation—the separation of rubber from the electrodes—occurs with repeated stress. Therefore, this negatively affects durability.

C. Developed Sensor Structure

In this study, we adopted a single-layer composite structure instead of the conventional double-layer structure by stitching electrodes (wires) into pressure-conductive rubber. We intended to keep the thin flexible property while improving durability with regard to the tangential force and deformation. Fig. 2 shows the structure of the sensor and a close-up photograph of the sensing element. As shown in the sensor part of the figure, a row of electrodes was configured in the horizontal direction by stitching electrodes (wires) into the front and back surfaces of the rubber, alternating back and forth, and then a column of electrodes was configured in the vertical direction as well. The sensing element was configured at the intersection of the row and column of electrodes. Beryllium copper wire (0.125-mm diameter) coated with gold was used for the electrodes. The wire was stitched at 3-mm intervals in the horizontal and vertical directions, as shown in Fig. 2. The stitch pattern was inscribed on the surface of the rubber before making the sensing element. Because the electrode wire was manually sewn with a needle, the wire position does not match the inscribed pattern as accurately as possible; there is a little dispersion at the production accuracy of the wire position. However, it would be possible to improve the accuracy, if a special jig or tool was utilized. Thus, by sewing the electrode, a preload between the wires at the wire junction occurs due to the wire tension in the sensing element. Therefore, it is necessary to make a sensor offset adjustment to compensate for the preload before any measurements are made. For the electrical isolation, because the electrode exists in both sides of the pressure-sensitive rubber, electrical insulation of both sides is necessary. Therefore, the artificial leather was attached to the back surface, and the surface was covered with a silicone rubber film. The thickness of the silicone rubber film is 0.1 mm. Throughout the experiment, which totaled about 100 h, there were no problems with the sensing functions caused by the silicone rubber film. But a long-term endurance experiment has not yet been carried out. Long-time durability experiments are necessary to test the sensor's usefulness in practical applications. Also, because the wires are coated with gold, there is no oxidation or chemical contamination. The thickness of the sensor was approximately 0.5 mm. Fig. 3 shows a fingertip with the tactile sensor. The intersection of the wires is the pressure-sensitive area. The sensor is 44-mm long and 12-mm wide. The sensing part is the 16×3 matrix with 3-mm pitch. When attaching the sensing part to the fingertip, in order to ensure improved mechanical strength and easy attachment to the fingertip, we used thread to sew the sensor on to elastic, artificial leather and attached this leather to cover the fingertip, as shown in Fig. 3.

D. Sensor Characteristics

Fig. 4 shows the relationship between the load and resistance of the sensor. To apply and remove pressure, a constant strain speed of 0.1 mm/s was adopted. The figure shows the results when pressure is repeatedly applied and removed for a total of five times. The characteristic of pressure sensitivity is in the range of 0–0.2 MPa.

However, the pressure-conductive rubber has a hysteresis effect, in which the relationship between stress and resistance values shows a loop at the time pressure is applied and removed.

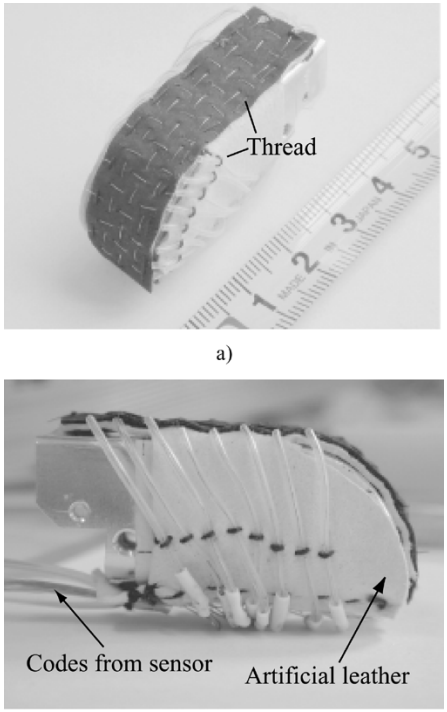

Fig. 3. Views of the fingertip. Tactile sensor array: 3 × 16 with 3-mm pitch. The size of fingertip: 44 × 12 mm.

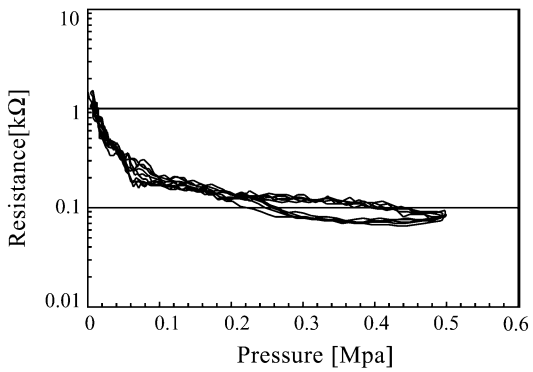

Fig. 4. Relationship between pressure and resistance of the sensing element.

As a result, the measured values differ from the loading sequence. Therefore, it is necessary to clarify the range of variation. As is known from the electricity-conducting mechanism in pressure-conductive rubber, the relationship between strain and resistance is important. Stress is related to resistance through strain. The fact that the stress-strain characteristic of this rubber causes a hysteresis effect was experimentally clarified by the authors [16]. The index for showing the degree of hysteresis is the ratio H/W, where H is the work lost due to hysteresis and W is the work per cycle, as shown in Fig. 5. The ratio (H/W) was measured experimentally by changing the frequency and applied strain. The results confirm that the ratio of (H/W) does not change up to about 10 Hz in frequency, as shown in Fig. 6. The experiment was also carried out by applying up to about 40% strain (almost the maximum value for the pressure-conductive rubber), but the H/W value did not change, as shown in Fig. 7. In other words, we confirmed experimentally that the

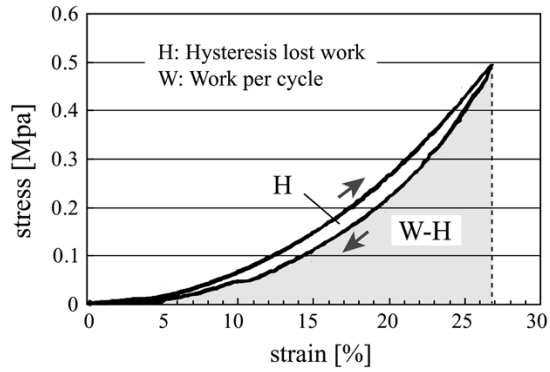

Fig. 5. Stress-strain characteristic of the rubber. (H) Hysteresis lost work and the (W) work per one cycle are shown.

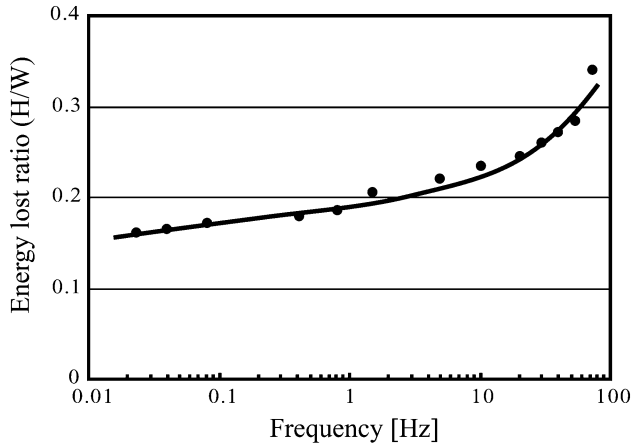

Fig. 6. Ratio of (H) hysteresis loss to (W) work load change due to load cycle frequency.

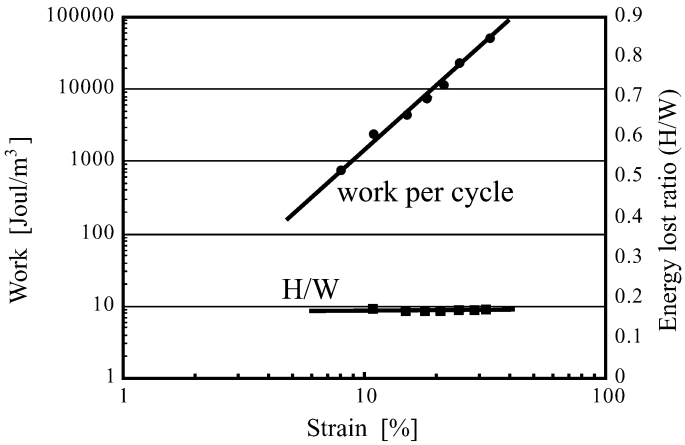

Fig. 7. (H) Ratio of hysteresis loss to (W) work load change due to strain.

hysteresis effect is not dependent on stress, and it is nearly constant at frequencies up to about 10 Hz. As a result, it was confirmed that the form of the hysteresis loop for each cycle did not change, even as cycles were repeated.

Generally, the endurance of pressure-conductive rubber is considered to be weak, but the rubber utilized in our study never changed its characteristics, even after loadings of one million cycles. In the experiment, we applied a repeated force (12 N) at 3 Hz to the rubber with a flat-head rod (diameter: 5 mm).

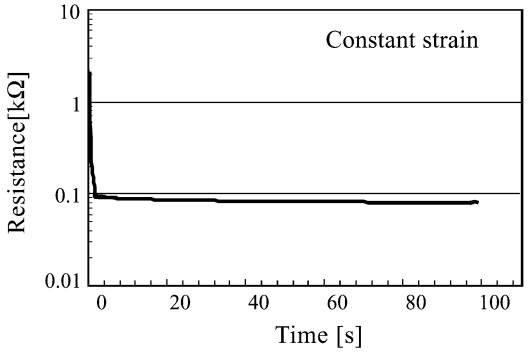

Fig. 8. Change of the resistance with time under constant strain condition.

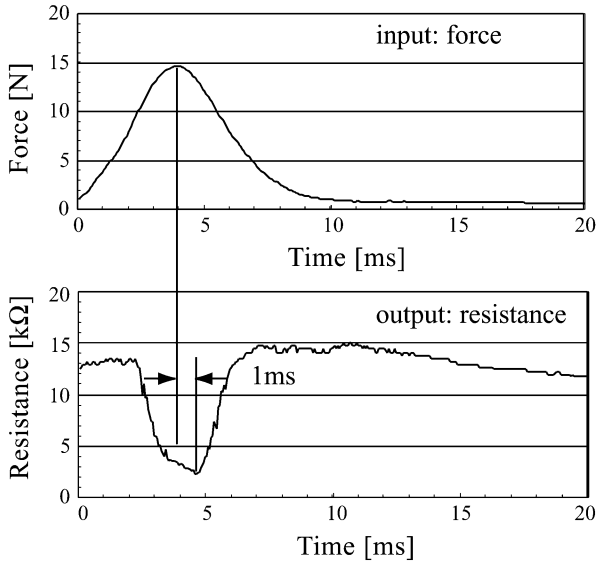

Fig. 9. Characteristics of time response. Relationship between force and resistance.

Then, the change in the resistance value was measured after repeated loading. No changes occurred with cyclic loading over one million times [9]. Fig. 8 shows the change of resistance with time when a constant strain is applied to the sensor. This measurement results from the creeping characteristic of visco-elastic materials such as rubber. Consequently, only a small change of resistance against a constant strain was observed during a measurement period of 100 s. Fig. 9 shows the time response. The upper part of the figure shows the waveform of the load applied to the sensor with an impulse hammer (PCB Piezotronics, Inc., impulse hammer GK291D), and the lower part shows the change of resistance during this time. The input load is given by striking the sensor element with the impulse hammer. The hammer contained a piezo-type load cell in the hammer head, which was 15 mm in diameter with a mass of 140 gw. Pressure-conductive rubber has a nonlinear characteristic between load and resistance, so the waveform of the input is different than the waveform of the output. Here, if the respective timing of peak values of both waveforms are compared, the delay is 1 ms. Therefore, the delay of the response between the input (load) and output (resistance) is estimated to be approximately 1 ms.

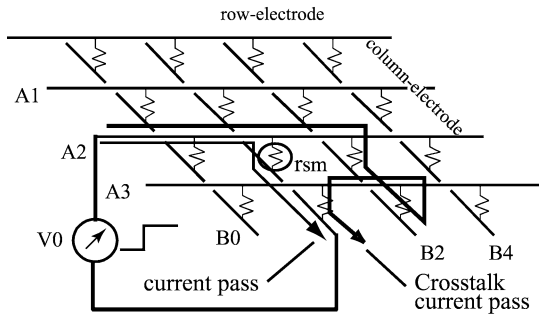

Fig. 10. Crosstalk between adjacent elements for arrayed sensing elements.

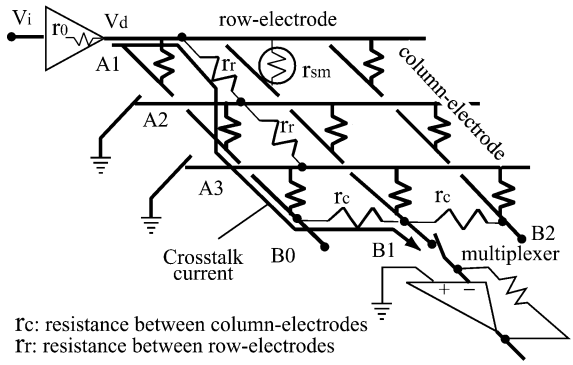

Fig. 11. Undesirable resistance exists between column and row electrodes.

III. Scanning Method

A. Previous Method

When adopting a sensor structure such as the one shown in Fig. 2, there are many crosstalk currents passing from sensing points other than the measurement point; these currents can interfere with measurement, as shown in Fig. 10. Four general methods of preventing these surrounding currents will be discussed next. 1) Ishikawa and Shimojo measured these respective elements completely independently [8]. However, by this method, field effect transistor (FET) switching is performed at every measuring point; therefore, it was difficult to achieve a thin and flexible measuring component. 2) Snyder *et al.* [10] proposed the method of preventing these crosstalk currents by inserting diodes at all of the measuring points. However, if the leak resistance (r_r, r_c) between electrodes shown in Fig. 11 exists, there are still crosstalk currents, and the size of the error in the measured values increases. Kanaya and Ishikawa prevented the crosstalk currents by cutting slits in the pressure-conductive rubber and inserting insulators between electrodes [12].

In addition, 3) Purbrick proposed the voltage mirror method [13]. This method eliminates crosstalk current passes by setting the drive lines that are not a consideration at the measuring point at a potential equal to the output voltage. Similar to this method, 4) Hillis proposed the zero potential method [14]. By changing the output circuit of the voltage mirror method, the voltage of the scanning electrodes is set to a zero potential. Using this method, instead of generating equal potential for the respective electrodes, the voltage is zero, and the circuit is simplified. However, Hillis used anisotropic electroconductive rubber. Therefore, only one operational amplifier is needed in order to cut the current passing nearby. However, leak resistance (r_r, r_c)

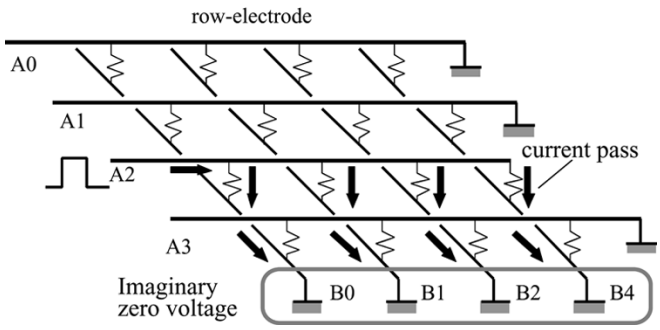

Fig. 12. Zero potential scanning method.

exists for the crosstalk current, as shown in Fig. 11 Therefore, we used the zero potential method by setting all drive lines (row electrodes), which do not involve the measuring point at zero voltage, and also by setting all output lines (column electrodes) at zero voltage. Since the input voltage of the operational amplifier must be at an imaginary zero voltage, operational amplifiers were connected to all of the columns. The column voltage then becomes zero.

B. Scanning Method

The scanning method used in this experiment is designed by taking the above points into consideration. In Fig. 12, the conceptual diagram of the scanning circuit is shown. The method used for row direction is similar to the method used so far: Voltage is applied to the row to be selected, and other rows are brought to zero voltage. As for column direction, operational amplifiers were connected to all of the columns, and all of the columns are brought to zero voltage. By doing this, the error in measurement due to leak resistance between electrodes can be excluded.

C. Errors Due to Scanning Circuit

1) Effeet of Output Resistance of Row Electrode Driver: The leak resistance is r_r between the row electrodes, connected in parallel. The synthesized resistance value of the row electrodes at drive line is r_{row}, as expressed in (1). r_0 is the output resistance of the operational amplifier of the row–electrode driver. The drive current, flowing where the voltage drop occurs in the row electrodes, and the voltage V_d at the drive points are expressed in (2)

$$\frac{1}{r_{\mathrm{row}}} = \sum_{j=1}^{N}\left(\frac{1}{r_{\mathrm{smj}}}\right) + \frac{1}{r_r} \tag{1}$$

$$V_d = \frac{r_{\mathrm{row}}}{r_0 + r_{\mathrm{row}}} V_i \tag{2}$$

where N is the number of columns and r_{smj} is the resistance value of the pressure-conductive rubber in the jth line of column electrodes. If the condition $r_{\mathrm{row}}i \gg r_0$ is satisfied, the circuit operates normally. However, when r_{row} approaches the output resistance r_o, the error on the measured values increases. Since this is caused by the lowering of the row electrode drive voltage, expressed as (2), it apparently appears as a lowering of the measured values.

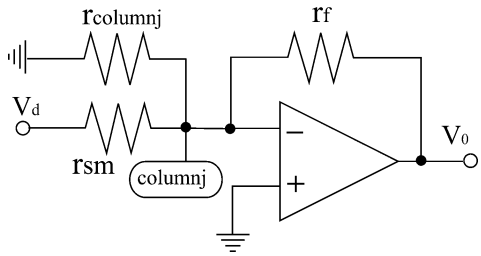

Fig. 13. Equivalent circuit for one column for the zero potential scanning method.

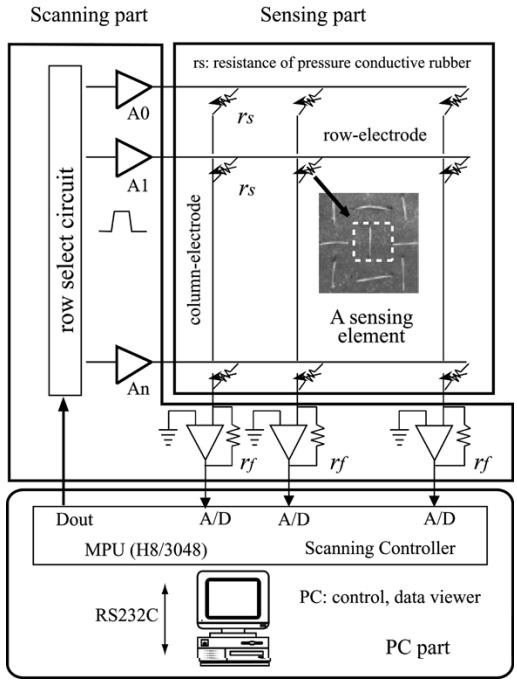

Fig. 14. Outline of sensor system. Sensing element, scanning circuit, PC controller, and data viewer.

2) Effect of Loop Gain of Operational Amplifiers: Fig. 13 shows the equivalent circuit when jth column of operational amplifiers is considered. $r_{\mathrm{column}}j$ represents the synthesized resistance of the resistance r_{sij} of the sensing element connected to the column electrodes and the leak resistance r_c between column electrodes. Since this circuit is a summing circuit, if the value of $r_{\mathrm{column}}j$ is not extremely low, the values of the resistance r_{sm} could be measured from the output. However, when the value of $r_{\mathrm{column}}j$ becomes extremely low, the lowering of the loop gain A_L, shown in (4), results, and problems appear, such as the deviation from the imaginary zero voltage at the input of operational amplifiers. β represents the feedback factor, and is expressed in (5)

$$\frac{1}{r_{\mathrm{column}}j} = \sum_{i\neq m}^{N}\left(\frac{1}{r_{\mathrm{sij}}}\right) + \frac{1}{r_c} \tag{3}$$

$$A_L = A \cdot \beta \tag{4}$$

$$\beta = \frac{r_{sm} r_{\mathrm{column}}j}{r_f(r_{sm} + r_{\mathrm{columnj}}) + r_{sm} r_{\mathrm{column}}j} \tag{5}$$

where A is the open-loop gain of the operational amplifiers and r_{sij} is the resistance value of the sensing element in the ith row

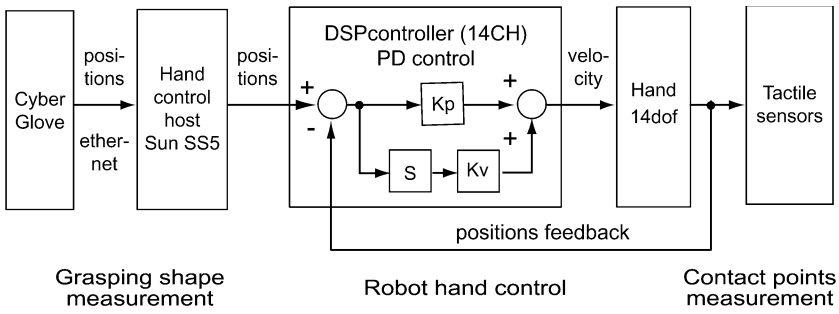

Fig. 15. Block diagram of the robot hand controller.

connected to the jth columns of the operational amplifier. m is the electrode number of the connected row, for which r_{sm} should be measured. In order to maintain the imaginary zero voltage under the condition of varying β, it is necessary to select the operational amplifiers having high open-loop gain over a wide frequency range. This time, OPA620 was used. It is a wide-band monolithic operational amplifier featuring a very fast settling time (25 ns), high output current drive capability (100 mA), and high gain bandwidth (200 MHz). There is also another condition. The output voltage of the operational amplifier must be within the source voltage. Therefore, it is necessary to satisfy (6)

$$V_{\text{Source}} \succ \left| \frac{r_f}{r_{sm}} V_i \right|. \tag{6}$$

This condition collapses when the value of r_{sm} becomes lower. Then, the zero voltage condition breaks and the crosstalk current appears; thus, r_f should be selected to satisfy (6).

IV. Sensor System

Fig. 14 shows the entire system. The system is configured by the a) sensor, b) scanning circuit, c) control, and d) PC. In the sensor, the electrode matrix was configured in the horizontal and vertical directions. The scanning circuit is configured in order to apply the zero electric potential method. The scanning controller controls the scanning circuit, based on command from the PC. The control was constructed of a one-board MPU (H8/3048). Scanning signals are generated using the DI/O port (16 bits) of MPU, and analog data is input from the sensor using the A/D converter (eight channels and 10 bits) of MPU. The PC displays measured data, adjusts the gain of each sensor element, and adjusts the offset due to the initial stress that occurs when the sensor is assembled. The PC is connected to the control (MPU) by an RS232C cable.

V. Robot Hand

The robot hand is shown in Fig. 1. The robot hand has four fingers. Each finger has three degrees of freedom (dof). In addition, the base of the thumb has one additional dof, and the palm has one additional dof. Thus, the robot hand has a total of 14 dof. Each finger is operated by a wire drive using dc motors as actuators. Each joint angle is measured using a potentiometer. In addition, each finger is equipped with a three-axial force sensor. The proportional plus derivative (PD) control method is used in joint angle control. The control block diagram is shown in Fig. 15.

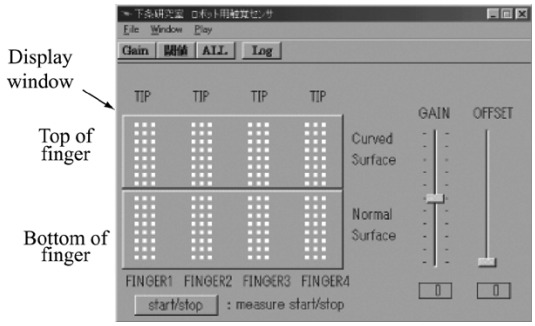

Fig. 16. Display and control windows. Left part is the measured data display window. Right part is the control window for adjusting offset and gain of each sensing element using scroll bars.

On the basis of data received from the CyberGlove, each joint angle of the robot hand is calculated. Each calculated joint angle is fed to the digital signal processor (DSP) controller as a position data, and the position feedback control is performed. The control cycle rate is 1 kHz. Moreover, each finger has compliance control in order to achieve flexible grasping [18]. Using the compliance control method, the command velocity $\boldsymbol{v}_d^h \in \mathbb{R}^{14}$ is computed as follows:

$$\boldsymbol{v}_d^h = K^h \left(\boldsymbol{\theta}_d^h - \boldsymbol{\theta}^h \right) - K^{hv} \boldsymbol{\theta}^h + K^{hf} \boldsymbol{F}^h \tag{7}$$

where $\boldsymbol{\theta}^h \in \mathbb{R}^{14}$ is the joint angle vector and $\boldsymbol{F}^h \in \mathbb{R}^{14}$ is the joint torque vector. The vector $\boldsymbol{\theta}_d^h \in \mathbb{R}^{14}$ is the desired angle positions for grasping. Matrices K^h, K^{hv}, and $K^{hf} \in \mathbb{R}^{14\times 14}$ are diagonal gain matrices.

VI. Grasping Experiment

In this experiment, the tactile sensor is attached on the surface of the fingers. As the robot hand grasped an object, such as a sphere or a column, the output of the tactile sensors were recorded. In addition, the transition of the position where the hand touched the object was measured according to the time-series data. Measured data was converted into 256 levels (8 bits) and displayed on the PC console.

Fig. 16 is a display window that indicates the measured data. The left portion of the window indicates the output of the tactile sensors on the four fingers. Each finger is configured by pressure display elements of three columns and 16 rows. The upper part corresponds to the top of the finger (eight rows), and the lower part corresponds to the bottom of the finger (eight rows). Each finger corresponds to a finger of the robot hand f1, f2, f3, and f4,

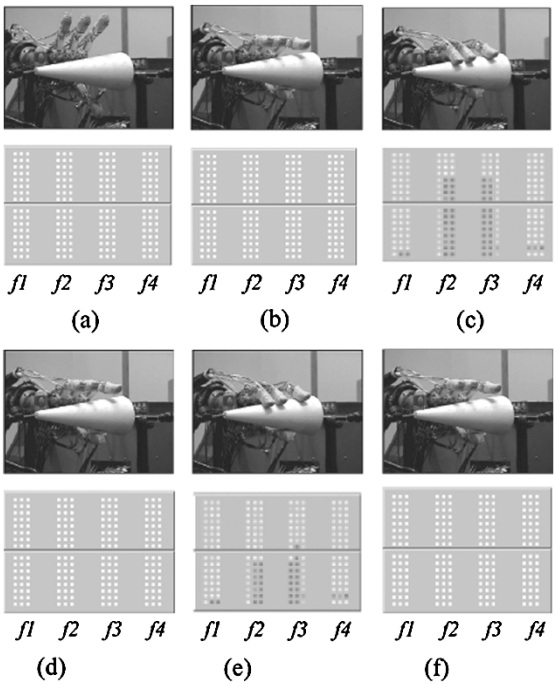

Fig. 17. Time-series transition data of tactile sensors when a cone-shaped object was grasped.

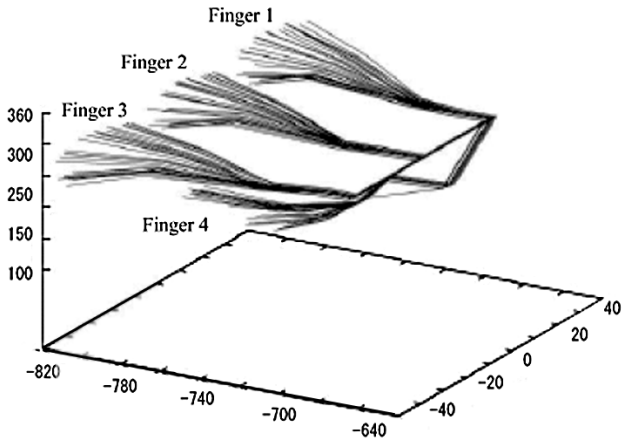

Fig. 18. Locus of each finger when a cone-shaped object was grasped.

as shown in Fig. 1. There is a scroll bar for adjusting the sensor parameters on the right side of the window. The user can select an individual sensor element and then adjust its gain and offset.

VII. Results and Consideration

Fig. 17 shows the time-series transition of contact points when a cone is grasped. Fig. 18 shows the locus of the robot hand when a cone is grasped. Fig. 17(a)–(f). sequences the operation of the robot hand and the display of tactile pressure distribution in the order of the time series. First, Fig. 17(a) and (b) represents the state when grasping the cone begins, so no touching could be confirmed at this stage. Fig. 17(c) represents the state when the cone is grasped. At this point, touching was detected around the bottoms of the fingers. Fingers f2 and f3 could especially confirm contact due to touching over a wider range than fingers f1 and f4. This is because the contact area of finger f1 is outside the sensing area. Fig. 17(d) shows that no touching could be confirmed because the hand was away from the cone. In Fig. 17(e), pressure was confirmed again, as in Fig. 17(c), and Fig. 17(f) shows the same results as Fig. 17(d). Grasping can be confirmed according to the time-series data of transition of these touching parts. Fig. 19 shows the distribution of grasping pressure when a sphere, column, and a human arm, which is an example of a flexible object, are grasped. The state of grasping was expressed correctly.

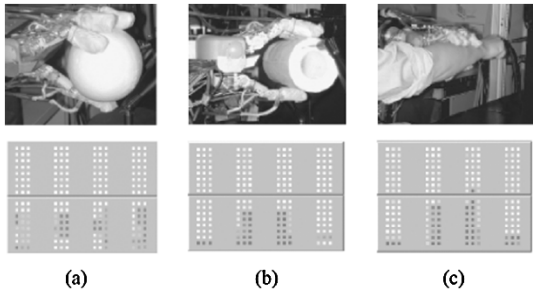

Fig. 19. Examples of the measured data when the hand grasped objects.

VIII. Conclusion

In this study, a thin, flexible sheet-like tactile sensor was developed. Instead of a conventional double-layer structure, a single-layer composite structure was adopted by stitching wire electrodes into pressure-conductive rubber. As a result, we were able to incorporate the advantages of a thin, flexible property, as well as improved durability against force and deformation. Sensor characteristics, such as sensitivity and time response, were described. Then, we attached the sensor to a four-finger robot hand and grasped a column, sphere, and so on, and showed the experimental data on the transition of the contact points characterizing the grasping operation.

Acknowledgment

The authors would like to thank R. Ikeda and T. Morioka for their help.

References

[1] V. J. Lumelsky, M. S. Shur, and S. Wagner, "Sensitive skin," *IEEE Sensors J.*, vol. 1, pp. 41–51, Feb. 2001.
[2] H. R. Nicholls and M. H. Lee, "A survey of robot tactile sensing technology," *Int. J. Robot. Res.*, vol. 8, no. 3, pp. 3–30, 1989.
[3] M. H. Lee and H. R. Nicholls, "Tactile sensing for mechatronics—A state of the art survey," *Mechatron.*, vol. 9, pp. 1–31, 1999.
[4] M. Inaba, Y. Hoshino, K. Nagasaka, T. Ninomiya, S. Kagami, and H. Inoue, "A full-body tactile sensor suit using electrically conductive fabric and strings," in *Proc. IEEE/RSJ Int. Conf. Intelligent Robots and Systems*, 1996, pp. 450–457.
[5] G. L. Soderhoim, "Sensing systems for touch and feel," *Design News*, pp. 72–76, Aug. 1989.
[6] "FSR Sensor," Interlink Electronics, Inc., 1997.
[7] M. Hakozaki, A. Hatori, and H. Shinoda, "A sensitive skin using wireless tactile sensing elements," in *Proc. Tech. Dig. 18th Sensor Symp.*, 2001, pp. 147–150.
[8] M. Shimojo, S. Sato, Y. Seki, and A. Takahashi, "A system for simultanious measuring grasping posture and pressure distribution," in *Proc. IEEE Int. Conf. Robotics and Automation*, Nagoya, Japan, 1995, pp. 831–836.
[9] "Pressure sensitive electric conductive elastomer," PCR Technical. [Online]. Available: http://www.scn-net.ne.jp/eagle/CSAEnglish.html.

[10] M. Ishikawa and M. Shimojo, "An imaging tactile sensor with video output and tactile image processing," in *Trans. SICE*, vol. 24, 1988, pp. 662–669.
[11] W. E. Snyder and J. S. T. Clair, "Conductive elastmers as sensor for industrial parts handling equipment," *IEEE Trans. Instrum. Meas.*, pp. 94–99, Feb. 1978.
[12] K. Kanaya and M. Ishikawa, "Tactile imaging system and its application," in *Proc. SOBIM*, vol. 13, 1989, pp. 45–48.
[13] J. A. Purbrick, "A force tranducer employing conductive silicone rubber," in *Proc. 1st Int. Conf. Robot Vision and Sensory Controls*, 1981, pp. 73–80. SOBIM, Vol. 13, no. 1, pp. 45–48, 1989.
[14] W. D. Hillis, "A high-resolution imaging touch sensor," *Int. J. Robot. Res.*, vol. 1, no. 2, pp. 33–44, 1982.
[15] D'T. Alessio, "Measurement errors in scanning of piezoresistive sonsor arrays," *Sens. Actuators*, pp. 71–76, 1999.
[16] M. Shimojo, M. Ishikawa, and K. Kanaya, "A flexible high resolution tactile imager with video signal output," in *IEEE Int. Conf. Robotics and Automation*, Sacramento, CA, 1991, pp. 384–391.
[17] M. Shimojo, "Mechanical filtering effect of elastic cover for tactile sensor," *IEEE Trans. Robot. Automat.*, vol. 13, pp. 128–132, Feb. 1997.
[18] A. Namiki, Y. Nakabo, I. Ishii, and M. Ishikawa, "High speed grasping using visual and force feedback," in *Proc. IEEE Int. Conf. Robotics and Automation*, 1999, pp. 3195–3200.

Makoto Shimojo received the B.E. degree in mechanical engineering from The University of Electro-Communications, Tokyo, Japan, in 1973, the M.E.Eng. degree from the Tokyo Institute of Technology, Tokyo, Japan, in 1976, and the Dr.Eng. degree from the University of Electronics Communications, Japan, in 1993.

From 1976 to 1992, he was a Senior Researcher at Industrial Products Research Institute, Tsukuba, Japan. From 1993 to 1997, he was a Senior Researcher at the National Institute of Bioscience and Human Technology, Tsukuba. From 1985 to 1986, he was a Visiting Scholar at Stanford University, Stanford, CA. From 1997 to 2001, he was a Professor of computer and information Ssciences at Ibaraki University, Japan. Since April 2001, he has been a Professor of mechanical engineering and intelligent systems at The University of Electro-Communications. His current research interests include mechatoronics, tactile sensing systems, and human interface using tactile information.

Akio Namiki received the B.E., M.E., and Dr.Eng. degrees in mathematical engineering and information physics from the University of Tokyo, Tokyo, Japan, in 1994, 1996, and 1999, respectively.

From 1999 to 2000, he was a Research Associate at the Japan Society for the Promotion of Science, Tokyo. Since 2000, he has been a Researcher at the Japan Science and Technology Corporation, Kawaguchi City, Japan. His current research interests include sensor fusion, robotic grasping, visual feedback, and active sensing.

Masatoshi Ishikawa received the B.E., M.E., and Dr.Eng. degrees in mathematical engineering and information physics from the University of Tokyo, Tokyo, Japan, in 1977, 1979, and 1988, respectively.

From 1979 to 1989, he was a Senior Researcher at Industrial Products Research Institute, Tsukuba, Japan. From 1989 to 1999, he was an Associate Professor with the Department of Mathematical Engineering and Information Physics, University of Tokyo, where, from 1999 to 2001, he was a Professor. Since 2001, he has been a Professor of information physics and computing at the University of Tokyo. His current research interests include parallel processing, smart sensors, vision chips, sensor fusion, robotics, and optical computing.

Ryota Makino received the B.E. degree in mechanical engineering from The University of Electro-Communications, Tokyo, Japan, in 2002. He is currently pursuing the M.S. degree in mechanical engineering and intelligent systems at The University of Electro-Communications.

Kunihiko Mabuchi was born in Japan in 1951. He received the M.D. and Ph.D. degrees from the Faculty of Medicine, University of Tokyo, Tokyo, Japan.

At the University of Tokyo, he worked on biomedical engineering as a Research Associate in the Institute of Medical Electronics, Faculty of Medicine, from 1986 to 1989, as an Associate Professor in the Research Center for Advanced Science and Technology from 1989 to 1996, and as a Professor in the Center for Collaborative Research from 1996 to 2002. Since 2002, he has been a Professor in the Department of Information Physics and Computing, Graduate School of Information Science and Technology, University of Tokyo, and his main research interests include the development of artificial organs, neural prostheses, the application of virtual reality techniques for medicine, and medical robotics.